Manufacturing studies and rf test results of the 1.3 GHz fundamental power coupler prototypes

Zhen-Yu Ma,[1,*] Hong-Tao Hou,[1] Shen-Jie Zhao,[1] Xu-Ming Liu,[1] Yu-Bin Zhao,[1] Sen Sun,[1] Ye-Liang Zhao,[1] Xiang Zheng,[1] Qiang Chang,[1] Hong-Ru Jiang,[1] Zi-Gang Zhang,[1] Kai Xu,[1] Xue-Fang Huang,[1] Yue-Chao Yu,[1] Ya-Wei Huang,[2] Li-Jun Lu,[1] Yan Wang,[1] Jing Shi,[1] Xiao-Han OuYang,[1] Wen-Feng Yang,[1] Xin-Yu Li,[1] Qiang Huang,[1] Chen Luo,[1] Hong Wu,[1] Xiao-Yun Pu,[1] and Chang-Hao Cheng[1]

[1]*Shanghai Advanced Research Institute, Chinese Academy of Sciences, Shanghai 201204, People's Republic of China*

[2]*ShanghaiTech University, Shanghai 201210, People's Republic of China*

(Received 27 July 2022; accepted 7 November 2022; published 15 November 2022)

The superconducting radiofrequency electron linear accelerator of the Shanghai HIgh repetition rate XFEL aNd Extreme light facility (SHINE) will use 600 TESLA-style cavities with 1.3 GHz fundamental power couplers for continuous-wave operation. The first batch of 26 1.3 GHz coupler prototypes has been fabricated from three domestic manufacturers for qualification. Several key manufacturing processes have been developed and qualified, including high residual resistivity ratio copper plating, vacuum brazing of ceramic windows, electron beam welding, and titanium nitride coating. In addition, uniform quality control and inspection processes have been established to ensure the power couplers meet the requirements for the intended use in the SHINE project. All the 1.3 GHz coupler prototypes have been power conditioned with 14-kW traveling wave and 7-kW standing wave rf in continuous-wave mode. Even higher power levels have been demonstrated with 20-kW traveling wave and 10-kW standing wave rf, which indicates their robustness.

DOI: 10.1103/PhysRevAccelBeams.25.113501

I. INTRODUCTION

The Shanghai HIgh repetition rate XFEL aNd Extreme light facility (SHINE) is a new continuous-wave (cw) hard x-ray free-electron laser (FEL) currently under construction in China [1,2]. The SHINE facility includes an 8-GeV superconducting linear accelerator (Linac), three undulator lines covering the photon energy range from 0.4 to 25 keV, three FEL beamlines, and the first ten experimental stations. The total facility length is 3110 m, and the tunnels are buried 29 m underground. Its goal is to become one of the most efficient and advanced FEL user facilities in the world, providing high-resolution imaging and other x-ray methods for cutting-edge research in diverse fields, including physics, chemistry, life science, materials science, and energy science.

The fundamental power coupler (FPC) is a crucial component of the superconducting cryomodules in the superconducting Linac. The main functions of FPC include transmitting a high radio-frequency (rf) power to the beam and providing isolation between atmospheric pressure in the waveguide and ultrahigh vacuum in the superconducting cavity through ceramic windows. It also has other functions such as temperature transition and coupling adjustment [3]. The SHINE Linac contains 600 1.3 GHz FPCs which are assembled in 75 superconducting cryomodules used for beam acceleration, and 16 3.9 GHz FPCs, which are assembled in two third harmonic superconducting cryomodules used for linearizing the longitudinal phase space before bunch compression [4,5]. The SHINE 1.3 GHz FPCs, which are used for cw operation, are modified and optimized based on the TTF-III coupler design developed at DESY for high power pulsed operation [6,7]. The main technical parameters of the SHINE 1.3 GHz FPC are listed in Table I. The 1.3 GHz FPC consists of four subassemblies: cold part, warm part, rectangular to coaxial waveguide conversion, and tuning mechanism, as shown in Fig. 1. The cold and warm parts each contain a ceramic rf window. On the vacuum sides of the ceramic windows, 10 nm of titanium nitride (TiN) is deposited to reduce the secondary electron yield (SEY) of the ceramic. The coupling to the cavity can be adjusted remotely by controlling the deformation of the bellows of the inner and outer coaxial conductors with a stepper motor. Some diagnostics ports are added for electron pickup and arc detecting in both the warm and cold parts. Except for the cold antenna, which is made of oxygen-free copper, the cold and warm parts are machined from stainless steel and plated with

*Corresponding author.
mazhenyu@zjlab.org.cn

TABLE I. Main technical parameters of the SHINE 1.3 GHz FPC.

Parameters	Specification
Operating frequency (GHz)	1.3
Type	Coaxial, double-rf-window
Ceramic rf window type	Cylindrical (cold) + Cylindrical (warm)
Maximum power (cw, SW) (kW)	7
External quality factor, Q_{ext}	4.12×10^7
Q_{ext} adjustment range	4.0×10^6–1.1×10^8
Antenna adjustment range (mm)	±7.5
Copper plating thickness (μm)	30/150, outer/inner coax
RRR of copper plating	30–80
TiN coating thickness (nm)	10

copper film to reduce rf loss in the coupler. There are four main differences with the original TTF-III design, which is basically the same as those used for the Linac Coherent Light Source (LCLS-II) facility couplers. The antenna of the cold part was shortened by 8.5 mm to achieve a higher external quality factor Q_{ext}. The copper plating thickness on the warm inner conductor was increased from 30 to 150 μm to alleviate overheating in the cw mode. The coaxial conversion waveguide is directly machined from a single block of aluminum, eliminating the rf matching posts and allowing for precision alignment. In addition, the capacitor ring used for the bias voltage was replaced by a copper flex ring to provide a better rf seal between the waveguide and coupler body. Four ports are added to the coaxial conversion waveguide of the SHINE 1.3 GHz coupler, one of which is used to detect the arc events of the warm window, one is used to measure the temperature of the warm window by an infrared sensor, and the other two are used as air cooling ports.

Advances in FPC development are often driven by project-specific requirements. The European X-ray Free Electron Laser (Eu-XFEL) required 800 1.3 GHz FPCs which work in pulse mode with an average power of 1.9 kW but peak power of 150 kW, and the LCLS-II required 280 1.3 GHz FPCs which work in cw mode with a maximum power of 7 kW [6,8,9]. To achieve the ultimate goal of mass production of 600 SHINE 1.3 GHz FPCs having equal and reliable quality, preliminary manufacturing studies of 1.3 GHz coupler prototypes began in May 2018. Three domestic manufacturers were chosen and different technical recipes were adopted, which is one of the major steps for the industrialization of couplers. To date, 26 1.3 GHz coupler prototypes have been fabricated and rf high power conditioned at the Shanghai Advanced Research Institute, Chinese Academy of Sciences (SARI, CAS). Also, nine of them have been assembled in the horizontal test cryomodules (HTC) with superconducting cavities and have been tested [10].

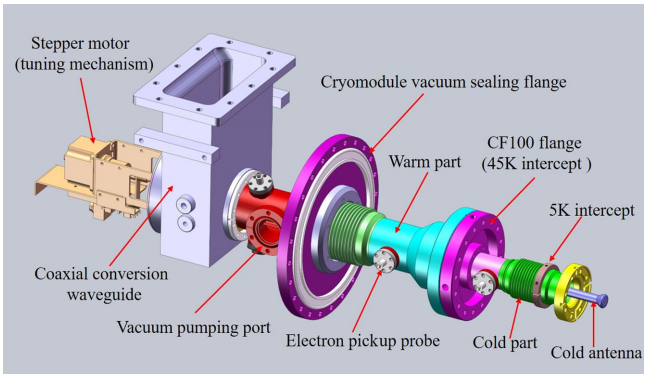

FIG. 1. Mechanical design of the SHINE 1.3 GHz FPC.

This paper is organized as follows: Section II presents the key manufacturing processes and their validation results for the SHINE 1.3 GHz couplers. The rf high power test results of the 1.3 GHz coupler prototypes are presented and discussed in Sec. III. Section IV gives the conclusions and outlook for the future.

II. MANUFACTURING AND VALIDATION PROCESSES

One SHINE 1.3 GHz FPC consists of 65 parts and requires 10 auxiliary tooling fixtures. The main steps in the 1.3 GHz coupler manufacturing are roughly the same as with other couplers of this type, such as the ones for the Eu-XFEL and the LCLS-II, including parts machining, brazing of subassemblies, copper plating of rf surfaces, TiN coating of ceramic windows, and electron beam welding (EBW) to form the final individual warm and cold parts [11]. The detailed coupler manufacturing processes are shown in Fig. 2. The cold and warm subassemblies are vacua brazed before electron-beam welding, which produces better reproducibility than just welding, allows more operator control, and is better for mass production. Cleaning, assembling onto the rf test stand, and vacuum baking are also essential for efficient rf high power conditioning [12]. Validation of every key manufacturing step not only provides a thorough understanding of the process but also improves product quality and reliability. Performance criteria and validation techniques need to be established for monitoring and controlling process parameters to ensure that the specified requirements continue to be met. Details about the qualification and validation of the key manufacturing processes are introduced below.

A. Vacuum brazing of ceramic rf windows

The 1.3 GHz SHINE FPC adopts a dual ceramic rf window structure, which is the weakest part of the coupler. The copper rings and ceramic windows are vacuum brazed together before TiN is deposited on the ceramic. The difficulty of this process lies in maintaining the concentricity between the

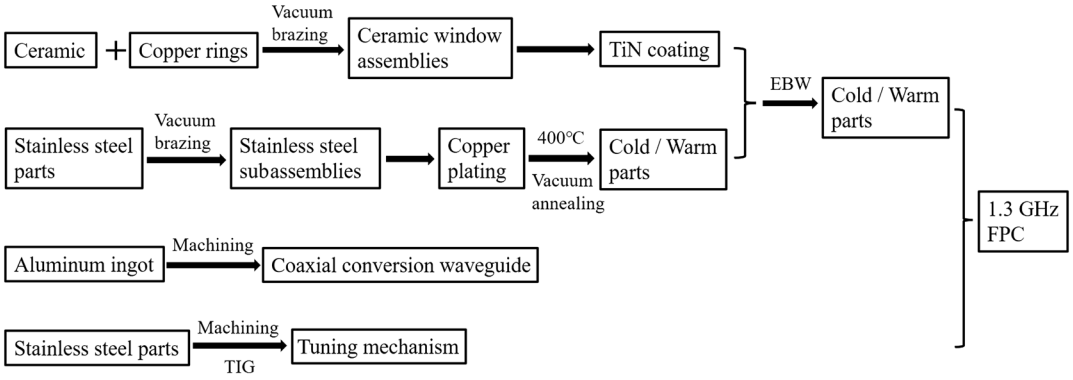

FIG. 2. The manufacturing process flowchart for the SHINE 1.3 GHz FPC.

copper rings and the ceramic window during the brazing cycle, which is caused by the different thermal expansion coefficient of copper and ceramic. Special tooling is adopted to ensure that the copper rings stay straight and do not become conical during brazing. In addition, shielding tubes are used to protect the ceramics from metallization from vaporized braze material. The brazing joints are 100% leak checked and the helium leak rate is required to be below 1.0×10^{-9} mbar l/s. Brazed warm and cold ceramic rf windows are shown in Fig. 3(a), and a microscopic picture of a ceramic-copper brazing joint is shown in Fig. 3(b). The diffusion of brazing material (type of CuAg) into the ceramic bulk is clearly seen. The width of the fusion zone at the ceramic-copper interface is approximately 20 μm, indicating the mutual diffusion of CuAg, Ni, and Cu elements.

The ability of the brazed ceramic rf windows to provide a vacuum seal at low temperature and high temperature was verified. A thermal cycle test was carried out 4 times from room temperature to 800 °C on brazed warm and cold ceramic rf windows, and the leak rate was less than 1.0×10^{-9} mbar l/s. A thermal shock test to 77 K from room temperature was also carried out 3 times, and the leak rate was less than 1.0×10^{-9} mbar l/s as well.

The tensile strength of the ceramic-copper brazing seams, required to be greater than 100 MPa, was further analyzed. First, three standard samples were pull tested on the RGM-4200 mechanical testing machine. The tensile loads were 18, 15, and 15.4 kN, and the corresponding tensile strengths were 146.7, 122, and 126 MPa, respectively, as shown in Figs. 4(a) and 4(b). Then, two warm ceramic rf windows and two cold ceramic rf windows were brazed with the optimized brazing parameters and pull tested for further validation, as shown in Fig. 4(c). The tensile strengths of the brazed ceramic rf windows are above 100 MPa and the results are listed in Table II.

B. TiN coating

Multipacting is a common phenomenon when rf power is fed into a vacuum environment [13]. The energy deposited by multipacting electrons can damage the ceramic rf windows. Surface layer properties affect the degree of multipacting, so after the ceramic rf windows are brazed, a TiN film is coated on the vacuum microwave surface of ceramic rf windows, which suppresses secondary electron emission [14]. The thickness of TiN coating is required to be 10 nm, and the acceptable range is 7–15 nm [15]. The

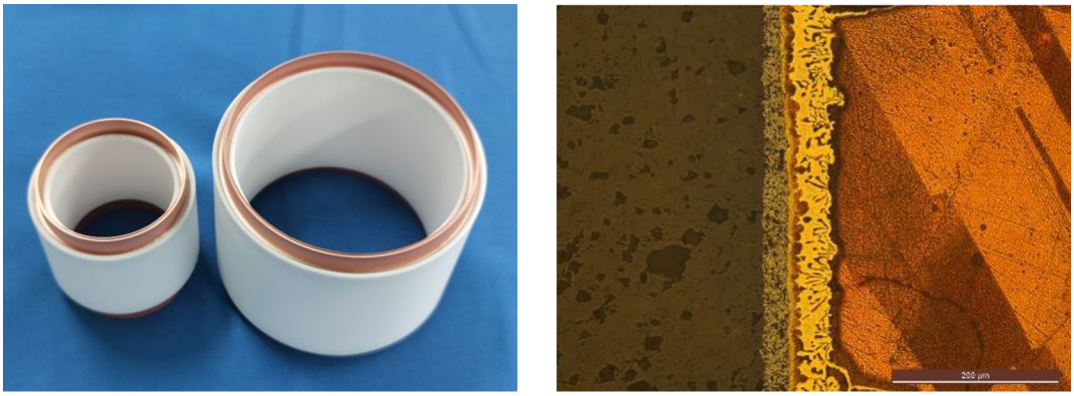

(a) (b)

FIG. 3. Warm and cold ceramic rf windows (a) and the microscopic structure of the brazing joint (b).

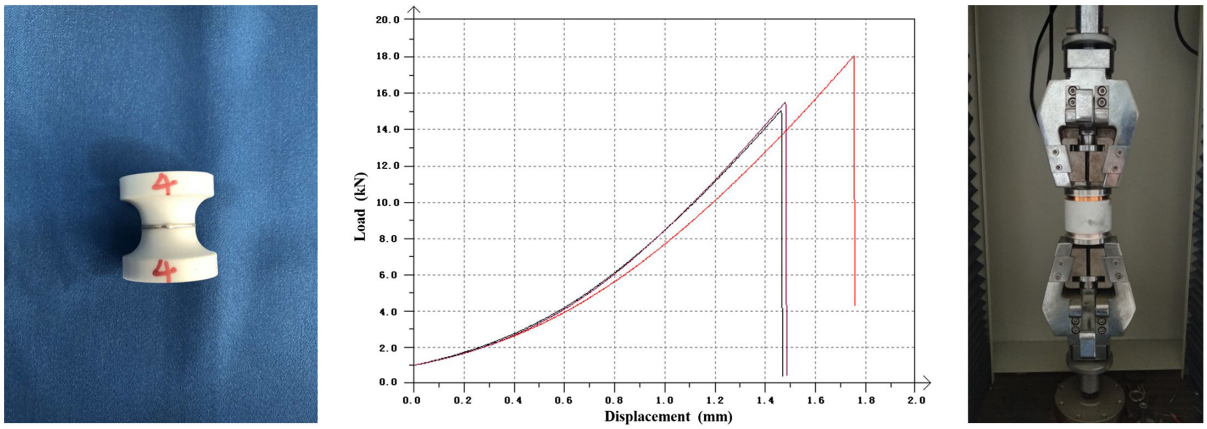

FIG. 4. A standard brazing sample (a) its tensile strength measurement curves (b), and a pull test of a ceramic rf window (c).

TiN film thickness, morphology, and chemical composition were investigated.

We use vacuum magnetron sputtering technology, which is a widely used method for film deposition. Due to the extremely small thickness of the TiN film and the large micropores on the ceramic surface, it is difficult to directly measure the thickness of the TiN film on the ceramic surface. To explore the TiN coating process, we used a quartz substrate instead of a ceramic substrate for the study of the samples. In order to measure the thickness uniformity of the TiN film on the surface of the ceramic window, glass slides were bound on the surface of the ceramic window. Samples were taken at 0°, 45°, 90°, 180°, and 270° along the circumferential direction, and upper, middle, and lower positions along the length of the window. There were 45 samples in total for the cold and warm ceramic windows, as shown in Fig. 5. The thickness measurement range of the TiN film inside the cold ceramic window was 12.2–13.6 nm, the range outside of the cold ceramic window was 12.7–13.4 nm, and the range inside the warm ceramic window was 11.4–12.2 nm. All meet the 7–15 nm technical requirement.

The chemical composition of the TiN film was determined by using x-ray photoelectron spectroscopy (XPS) analysis. XPS spectra were measured on "as received" samples and after each ion bombardment that removed a layer of material. Table III lists the contents of the main atomic constituents of the film and the Ti:N ratio at different depths from the starting sample surface, which suggests that the proportion of titanium and nitrogen atomic content is close to 1.08 in the depth range of 7–15 nm, and the oxygen content mainly comes from the base material.

X-ray diffraction (XRD) analysis was also performed to study the film stoichiometry. For an XRD analysis, the TiN film should be thick enough (some hundreds of nanometers) to be characterized, and an alumina substrate was used to improve precision. Figure 6 shows the comparison of the actual XRD measurement results of the TiN film (red line) with the standard TiN spectral pattern (blue line). The agreement between them is as high as 94%.

Measurements of SEY as a function of primary electron energy were performed on three types of samples: an uncoated ceramic sample, a TiN-coated ceramic sample, and a TiN-coated ceramic sample with 650 °C baking, as shown in Fig. 7. It is clearly seen that the maximum SEY value decreases from 7.2 to 1.8 as a result of the TiN coating, but the high temperature baking increased the maximum SEY from 1.8 to 2.2. In addition, high temperature baking will also cause Ti to diffuse into the ceramic bulk, resulting in increased dielectric loss and blackening of the ceramic surface. This is why the high temperature brazing process is no longer performed after the TiN coating of the ceramic window, and EBW was chosen as the final process.

C. Copper plating

In order to reduce the rf loss, a copper film is plated on the stainless-steel microwave surface of the couplers. The optimum characteristics of the copper plating layer are a

TABLE II. Tensile strength results of ceramic rf windows.

	Sample	Maximum Load/kN	Tensile strength/MPa
1	Warm ceramic rf window-1	28.5	132.95
2	Warm ceramic rf window-2	27.3	127.33
3	Cold ceramic rf window-1	16.0	125.42
4	Cold ceramic rf window-2	16.5	129.47

FIG. 5. The TiN film thickness measurement positions on the ceramic rf windows.

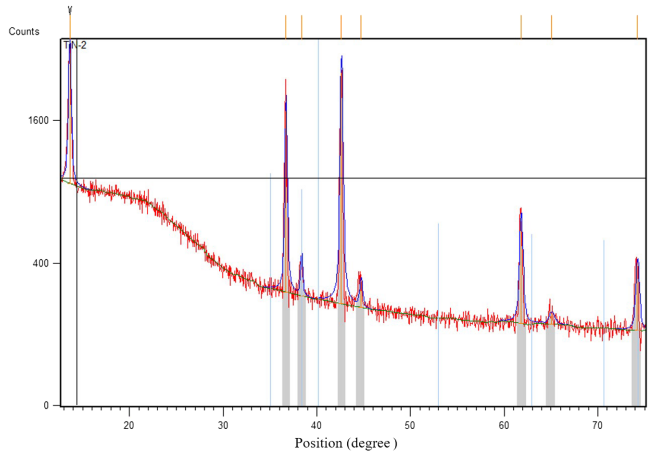

FIG. 6. XRD patterns for comparison between the real TiN film and standard TiN.

compromise between rf and thermal performance [16]. The copper plating process is the most challenging and trickiest step for coupler manufacturing due to the complicated geometries of some parts (bellows, conical parts, and big flanges) and the very demanding specifications. There are three common copper electroplating technologies, namely acid sulfate copper plating, cyanide copper plating, and pyrophosphate copper plating. Sulfate copper plating is our primary copper electroplating process because of its large current density and fast plating speed, which is beneficial for thicker copper film. Although cyanide copper plating has better copper film density, it is not adopted due to its toxicity and low current efficiency. The copper thickness specifications for the SHINE couplers are basically the same as those used for the LCLS-II couplers [17]. The thickness and tolerance of the copper films on the warm outer conductor and cold outer conductor are 30 μm ± 20% on tubular parts and ±30% on the bellows. The warm inner conductor thickness and tolerances are 150 μm ± 20% on tubular parts and 150 μm ± 30% on the bellows. The RRR value specification is 30–80 after baking at 400 °C for 1.5 h under vacuum.

Samples of different geometries were copper plated and tested for technical qualification. Bellows were most difficult to electroplate uniformly and to achieve the specified thickness because of their high aspect ratios. Some special tools were designed and tested with careful optimization to achieve the uniformity goal. The samples for the copper film thickness measurements were cut out with special cutting blades to prevent overheating the material. Each sectioned part was embedded with epoxy resin, ground, and polished thoroughly until a high-quality final surface appears. Figure 8 shows the thickness measurements of the copper films for three types of coupler bellows. For the cold and warm outer conductor bellows, the measured values of 21–34.6 μm are well in the specified range of 30 μm ± 30%, and the measured values of 105.2–178 μm are also well in the specified range of 150 μm ± 30% for the warm inner conductor bellow.

The RRR is defined as the ratio of the electrical resistivity of the material at 0° C ($T = 273$ K) and the residual electrical resistivity measured at the liquid helium boiling point ($T = 4.22$ K). Furthermore, the room temperature (i.e., $T = 300$ K) electrical resistivity is weakly dependent on the material purity [18]. Consequently, we adopted the following expression for RRR:

$$\mathrm{RRR} = \frac{\rho(T = 300\ \mathrm{K})}{\rho_R}.$$

TABLE III. The chemical composition of TiN surface layer.

		Atomic content %				
Etch time (s)	Etch depth (nm)	C	O	Ti	N	Ti:N
0	0	18.08	36.24	24.04	21.64	1.11
50	6	1.06	32.8	34.64	31.5	1.09
150	18	0.43	31.21	35.45	32.91	1.07
400	48	0.38	31.01	35.29	33.32	1.05

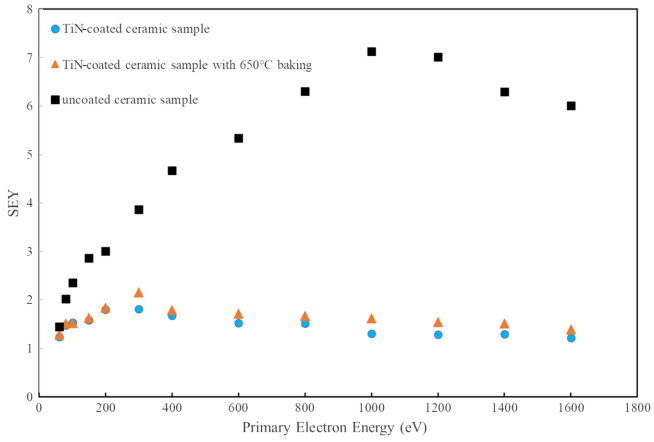

FIG. 7. SEY versus primary electron energy.

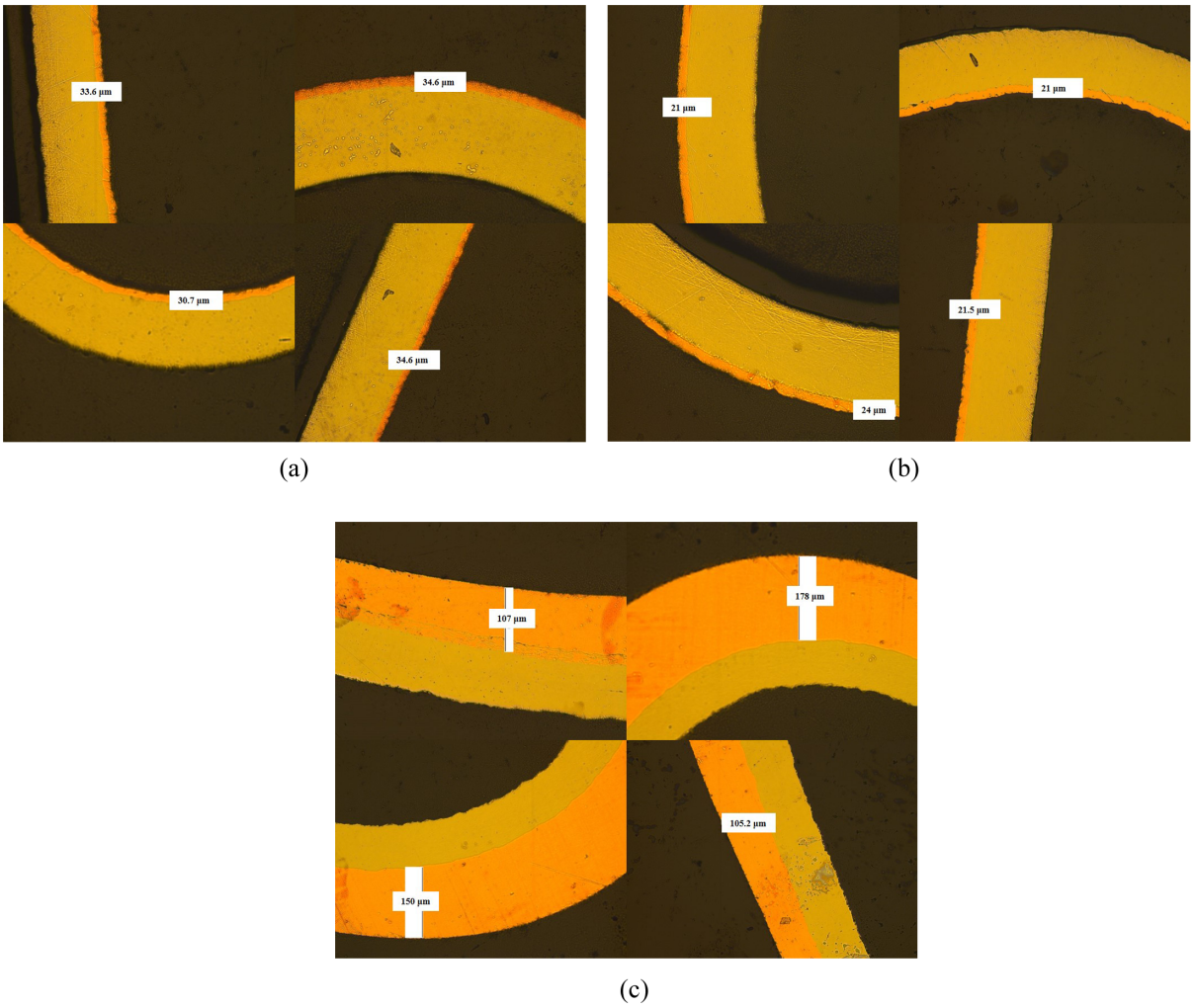

FIG. 8. Thickness measurements of the copper films for (a) warm outer conductor bellow, (b) cold outer conductor bellow, and (c) warm inner conductor bellow.

Six samples used for RRR measurements were cut from two actual coupler prototypes, representing the cold outer conductor, warm outer conductor, and warm inner conductor, as shown in Fig. 9. Due to the size limitation of the test device container, the sample size was required to be less than 100 mm in length and less than 5 mm in width, including the bellow and its straight sections at both ends. It is believed that the measurements of such samples were more accurate than those of simple flat samples and more representative of the actual RRR values of the coupler copper film. The RRR measurement results are listed in Table IV. The measured RRR values of 56–75 are well within the specified range of 30–80 and there is good reproducibility for 30 and 150 μm copper films.

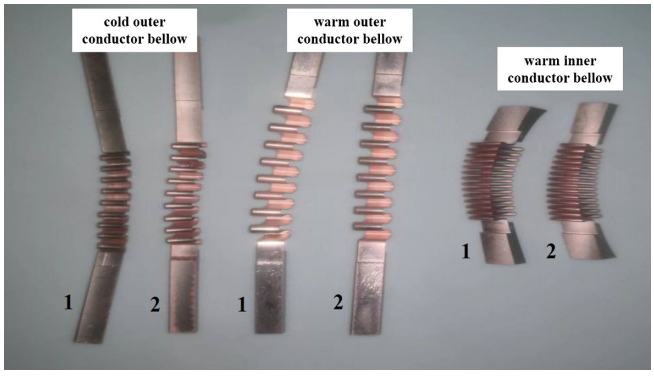

FIG. 9. Samples used for RRR measurements of the cold outer conductor, the warm outer conductor, and the warm inner conductor.

Fatigue tests were carried out on warm inner conductor bellows and warm/cold outer conductor bellows with and

TABLE IV. RRR measurement results for three sections from 1.3 GHz coupler prototypes.

	Cold outer conductor		Warm outer conductor		Warm inner conductor	
No.	1	2	1	2	1	2
RRR	75.1	75.1	59.7	68.4	60.6	56.2

FIG. 10. Fatigue test of a 1.3 GHz coupler bellow.

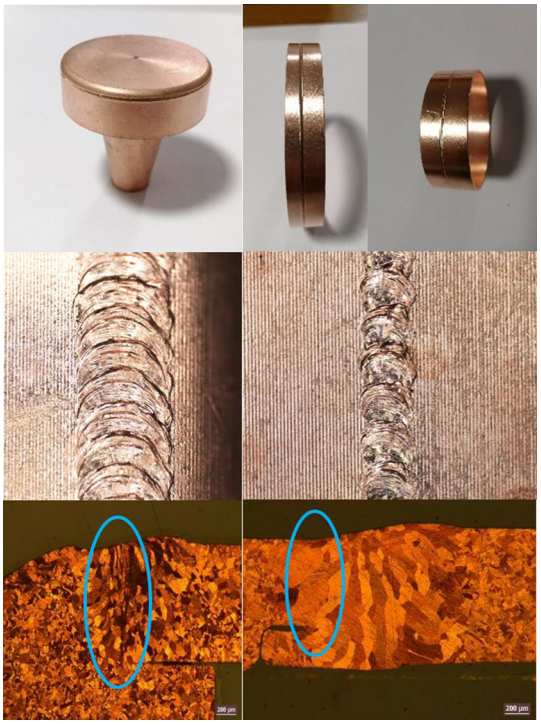

FIG. 11. EBW samples and photos of the electron beam welds.

without copper coating, with repeated movements of ±7.5 mm, as shown in Fig. 10. All of them ruptured after 10,000 cycles, and the fatigue times of the copper-coated bellows were slightly smaller than those of the copper-uncoated bellows (see Table V). Thus, the copper plating process did not have a great impact on the quality of the bellows.

In addition, adhesion tests were done to determine the quality of the copper film. These checks were done after ultrasonic cleaning, 2000 psi high pressure water rinsing, and thermal immersion at 77 K from room temperature. Cleanliness verifications were done using a millipore membrane filter after each ultrasonic bath and high-pressure rinse to check for particulates that flake off. No copper film peeling or copper particles were found during these tests.

The magnetic permeability of the coupler is required to be less than 1.05 to reduce the influence of the magnetic field on the superconducting cavity. It was found that the thickness of the nickel layer had a non-negligible effect on the magnetic permeability. When the thickness of the nickel layer was controlled to be within 1.0–1.5 μm, the magnetic permeability after copper plating was below 1.02, and the magnetic permeability after 400 °C annealing was below 1.03.

D. Electron beam welding

Once the subassemblies were fabricated, the integration of ceramic window, inner conductor, and outer conductor were done by EBW for the cold and warm parts. Sophisticated fixtures were designed to protect the ceramic windows from being metalized by the welding vapor during EBW and could be dismounted easily without harming the copper films of the coupler. No weld beads were allowed inside the coupler and smooth electron beam welds were necessary for good performance.

The EBW of the copper coupler parts involves two welding setups. One is for welding the copper ring to the inner conductor; the other is for welding together the two copper rings. The welding structure of the two copper rings adopts step interlocking, which can be better positioned and is different from that used for the Eu-XFEL and the LCLS-II couplers. Samples were first tested to determine

TABLE V. Fatigue test results for 1.3 GHz coupler bellows.

	Cold outer conductor bellow		Warm outer conductor bellow		Warm inner conductor bellow	
	Cu uncoated	Cu coated	Cu uncoated	Cu coated	Cu uncoated	Cu coated
Cycles to failure	10 165	10 119	10 054	10 034	10 119	10 039

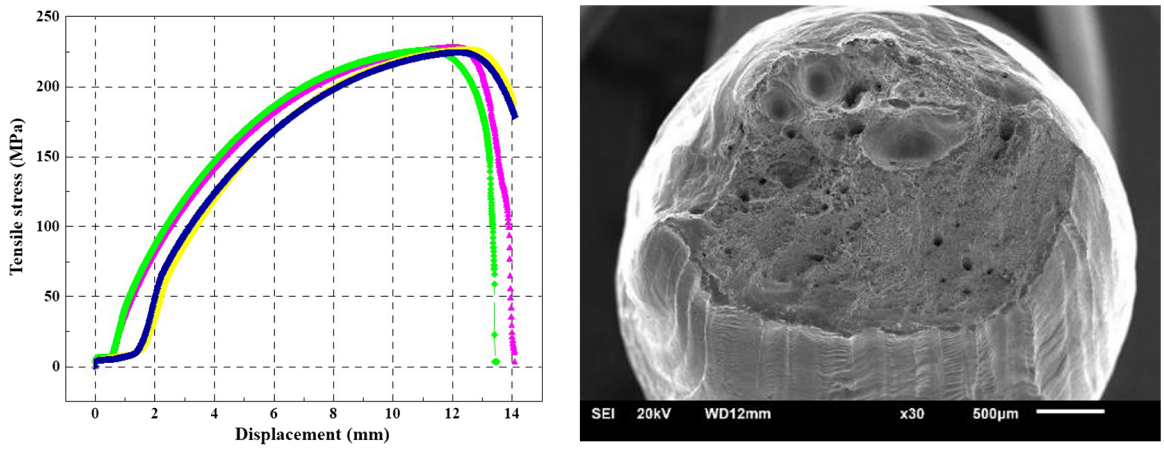

(a) (b)

FIG. 12. The tensile strength tests of the welded samples (a) and a cross section of a fracture (b).

the electron beam current and penetration. A good weld surface was formed as shown in Fig. 11, characterized by the uniform size of the fish scale pattern of the weld, the absence of surface defects, and the uniform width of the weld. The penetration depth of the first weld type is controlled to 1 mm while the penetration depth of the second welding structure is controlled to 0.7 mm.

The welded samples were helium leak tested and the leak rate was better than 1.0×10^{-9} mbar l/s. Four samples were then pull tested to determine their tensile strength. The weld joint narrowed when stretched, and the fracture morphology was characteristic of a dimple fracture, meaning that the weld joint deformed plastically, as shown in Fig. 12. The average tensile strength of the weld joints was 226 MPa, close to that of the base metal material.

In the actual EBW process for the couplers, the temperature of the first structure was 63 °C, the temperature of the second structure was 75 °C, and the maximum temperature of the ceramic window was about 283 °C, which is much lower than the brazing temperature and the oxidation temperature of TiN film. Therefore, the temperature increase generated by EBW did not affect the properties of the TiN film on the ceramic windows.

III. RF HIGH POWER TESTS

The FPCs need to be fully rf high power conditioned at room temperature prior to installation on the superconducting cavities that are used in the cryomodules. An rf high power test is the most direct and effective means to verify whether the manufacturing processes of the FPCs and their performance meet the design targets. Also, the conditioning removes residual absorbed gases and burns-off microscopic surface imperfections.

A. Surface treatments and assembling procedures

The surface treatments and assembling of the FPCs need to be done correctly to make the rf conditioning faster and more efficient. All the coupler parts were delivered into the clean room and visually inspected with an endoscope to check the quality of the internal welds, braze joints, and copper-plated surfaces. The coupler parts were first cleaned in an ultrasonic bath with a solution of detergent in the class 100 cleanroom, then rinsed with ultrapure water until the resistivity of the drained water exceeded 14 MOhm cm in the class 10 cleanroom. All rinsed coupler parts were blown using filtered high-purity nitrogen gas and left to dry overnight under the laminar flow in the class 10 cleanroom. Before assembling, each coupler part was blown with filtered high-purity nitrogen gas again in conjunction with a particle counter. The count was required to be less than ten particles of size >0.3 microns per cubic foot; if not, the coupler parts were returned to the ultrasonic bath. The pumping assemblies (ion pumps, metal angle valves, and gauges) were mounted on each warm part and on a rectangular waveguide on which two cold parts are mounted for testing. Then, a leak test was performed for both the warm parts and the cold assembly. Once the tightness was verified, the FPCs were baked out in a modified vacuum furnace at 150 °C for 72 h. Baking served to expel the adsorbed hydrogen, water, and organic compounds. After baking, the vacuum pressure of the cold assembly was required to be less than 5×10^{-9} mbar, the vacuum of the warm parts was required to be less than 5×10^{-8} mbar, and the overall leak rate of the cold assembly and warm parts was required to be less than 1.0×10^{-9} mbar l/s. Also, a residual gas analyzer (RGA) was used to verify that the H partial pressure was less than 5×10^{-9} mbar, the H_2O partial pressure was less than 5×10^{-10} mbar, and the partial pressure of each gas with a mass number greater than 44 was less than 5×10^{-12} mbar.

B. Coupler test setup and rf conditioning procedures

The rf test system for the 1.3 GHz FPCs consists of four major subsystems: (1) power source system, (2) power

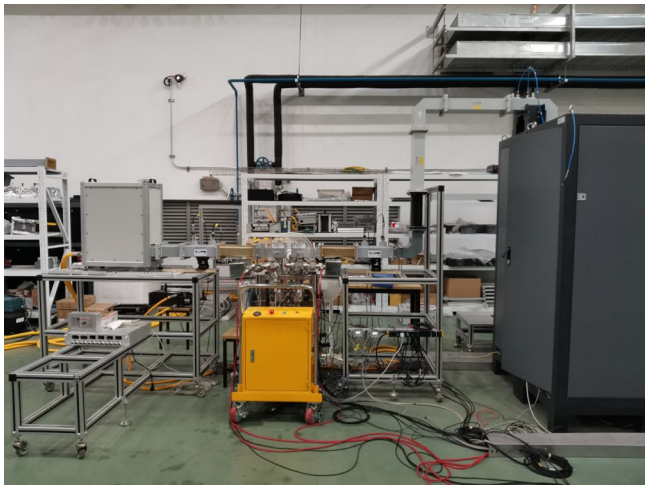

FIG. 13. The layout of rf test system for 1.3 GHz FPCs.

transmission system, (3) test bench, and (4) interlock control and data acquisition system [19,20]. The layout of rf test system is shown in Fig. 13. The power source system consists of a solid-state amplifier (SSA) capable of producing 30 kW of cw power. The power transmission system includes various transmission waveguides, circulators, water-cooled rf-absorbing loads, and movable waveguide shorts. The test bench connects a pair of couplers through a rectangular waveguide. A data acquisition system monitors incident power, reflected power, temperatures, vacuum levels, electron-probe currents and arc detector signals, and a protection interlock system shuts off the power immediately if particular signal thresholds are exceeded.

The rf conditioning procedure consists of three conditioning steps. During the first step, the rf pulse length is first set to 1 ms, and the power is increased in increments of 1 kW every 5 min from 1 to 28 kW in traveling wave (TW) mode. The same operation is then repeated with 2, 4, 8, 15, and 20 ms long pulses. The pulse repetition frequency is 10 Hz. During the second step, the power is switched to cw mode and increased in steps of 0.5 kW every 20 min from 1 to 14 kW, then the power is kept at this level for 6 h. For the third step, the rf load is replaced with the movable short for standing wave (SW) operation. In this case, the power is increased in steps of 0.5 kW every 30 min from 1 to 7 kW, then the power is kept at this level for 12 h. During the rf power conditioning, the vacuum levels and the electron-probe currents in the FPCs are monitored and kept under specific thresholds by managing the power increment. Other parameters are also monitored during rf conditioning for safety, such as reflected power, ceramic window temperatures, and arc detector signal levels.

The basic methodology of rf high power condition is to perform pulse conditioning first and then cw conditioning, and switch to pulse conditioning if cw conditioning encounters problems. Any increase of vacuum close to the threshold results in a power reduction. For vacuum events exceeding 5.0×10^{-6} mbar, the rf power is cut immediately and recovered when the vacuum pressure is lower than 1.0×10^{-7} mbar. The choice of the interlock threshold is a compromise between establishing a safe procedure and avoiding lengthy conditioning [21]. For example, the interlock threshold of the vacuum at the beginning is 1.0×10^{-6} mbar and then increased to 5.0×10^{-6} mbar to speed up rf conditioning without harming the couplers. The interlock threshold of the warm window of the coupler is 80 °C based on the past experience [22].

C. rf power test results

To date, 26 1.3 GHz FPC prototypes from three domestic manufacturers have been manufactured and rf high power conditioned manually. All of them have successfully passed the rf high power tests on the room temperature test bench, including cw operation at 14 kW for 6 h in TW mode and cw operation at 7 kW for 12 h in SW mode. A paper on the details of the rf test results has been published [10]. There was a noticeable variation in the rf conditioning times, ranging from 72 to 200 h. Also, it was found that the coupler insertion loss decreased from 0.092 dB before conditioning to 0.046 dB after conditioning. Variations resulting from different manufacturing procedures may be one reason. To understand the reason, and to further reduce the rf conditioning times, further studies will be done. In addition, an automatic rf test bench has been installed at SARI and is being used. It is worth noting that the average conditioning time of a new batch of 10 1.3 GHz FPCs, recently manufactured by one of the manufacturers, has been greatly shortened with the maturity of the manufacturing processes, surface treatments, and assembling procedures, and can be controlled at about 50 h on the automatic rf test bench with the same rf conditioning methodology.

Past studies suggest that the original TTF-III coupler design could operate reliably up to 5 kW cw in SW mode [22]. A LCLS-II 1.3 GHz coupler prototype was rf conditioned up to 6 kW in the horizontal test stand cryostat [23]. The SHINE cw 1.3 GHz coupler prototypes, which were modified in the same way as the 7 kW LCLS-II couplers, have demonstrated 7 kW operation in SW mode, and some have been operated at higher power.

Below, we describe a series of rf tests with the SHINE 1.3 GHz coupler prototypes to determine the cw power limit. Starting in cw TW mode, the rf power was increased in steps of 0.5 kW every 10 min from 1 to 20 kW, and then the power was kept at this level for 12 h. The maximum temperature of the outer surface of the couplers did not exceed 65°, and it remained basically stable during the 12 h. The vacuum level in the warm parts and the cold assembly remained below 1.0×10^{-6} mbar and slowly decreased. Figure 14 shows the temperature distributions of the upstream coupler and downstream coupler at different rf

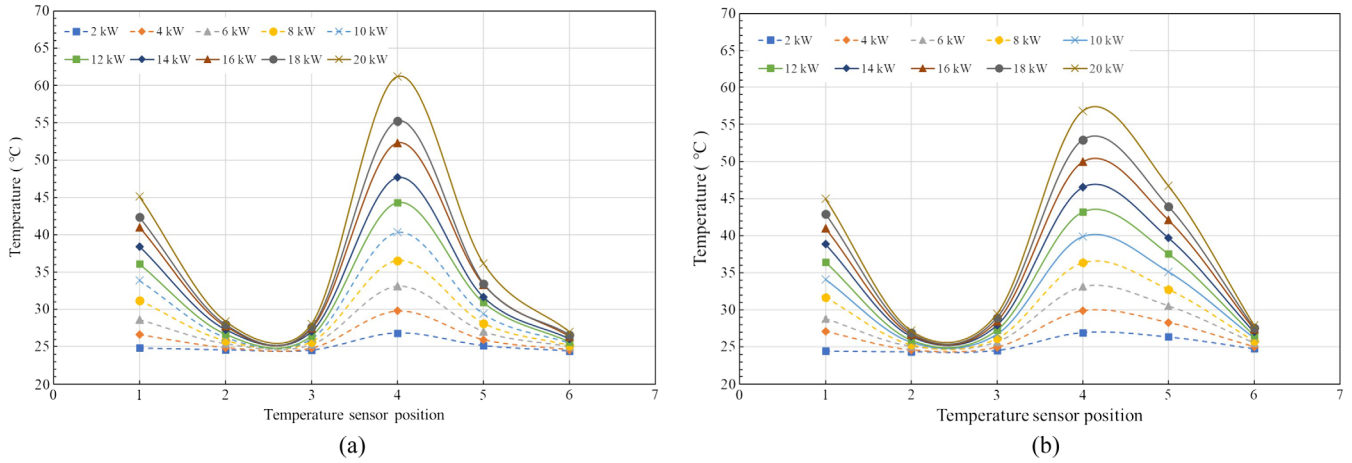

FIG. 14. Temperature distribution of FPCs with the rf power ranging from 2 to 20 kW in TW mode for the upstream coupler (a) and the downstream coupler (b).

power levels. The temperature probes were distributed on the surface of the coupler along the axial direction where the temperature of position 1 refers to the infrared temperature of the coupler's warm window, and position 4 refers to the CF100 flange of the cold part, which is close to the cold window. Figure 15 shows the change of coupler vacuum pressures with increasing power and the trend during the 12 h of operation at a constant power of 20 kW.

The rf high power test setup was then changed to SW mode and pulsed rf conditioning was first performed, followed by cw rf conditioning. The rf power was increased in steps of 0.5 kW every 30 min from 1 to 10 kW in cw mode, then the power was kept at this level for 12 h. Figure 16 shows the temperature distribution for the upstream coupler and downstream coupler at different rf power levels. The maximum temperature of the couplers did not exceed 70°. The difference between the maximum temperature of the upstream coupler and the downstream coupler was due to the different node locations of the SW along the FPCs. The vacuum levels in the warm parts and the cold assembly were lower than 1.0×10^{-6} mbar and remained stable during the 12 h, as shown in Fig. 17.

Figure 18 shows the history curves of vacuum pressure versus rf power throughout the rf tests. During the rf conditioning, a total of 22 interlock events occurred, mainly vacuum interlocks and arc interlocks, but no events occurred during the final 12 h of operation at fixed power. Specifically, there were ten arc and ten vacuum interlock events in the warm parts of the upstream and downstream couplers, and only two vacuum interlock events in the cold assembly. The factors that ultimately limited the rf conditioning were the intense degassing and arcs in the warm parts of the FPCs, which caused vacuum spikes above the interlock threshold. It should be noted that during the rf

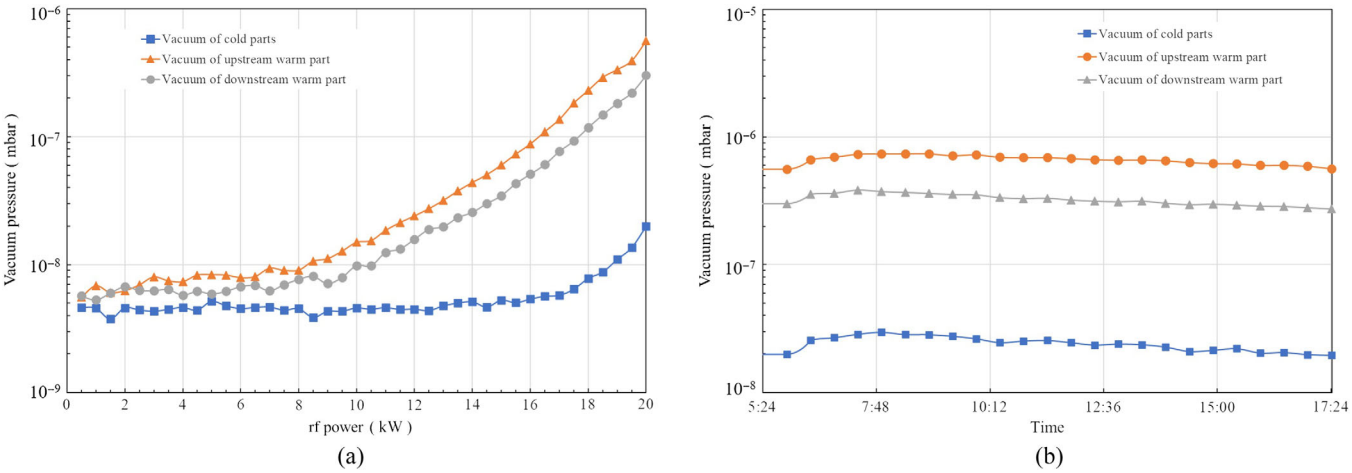

FIG. 15. The vacuum pressure of the warm part and cold assembly with the power ranging from 1 to 20 kW in TW mode (a), and the vacuum pressure variation during the 12 h of operation at 20 kW (b).

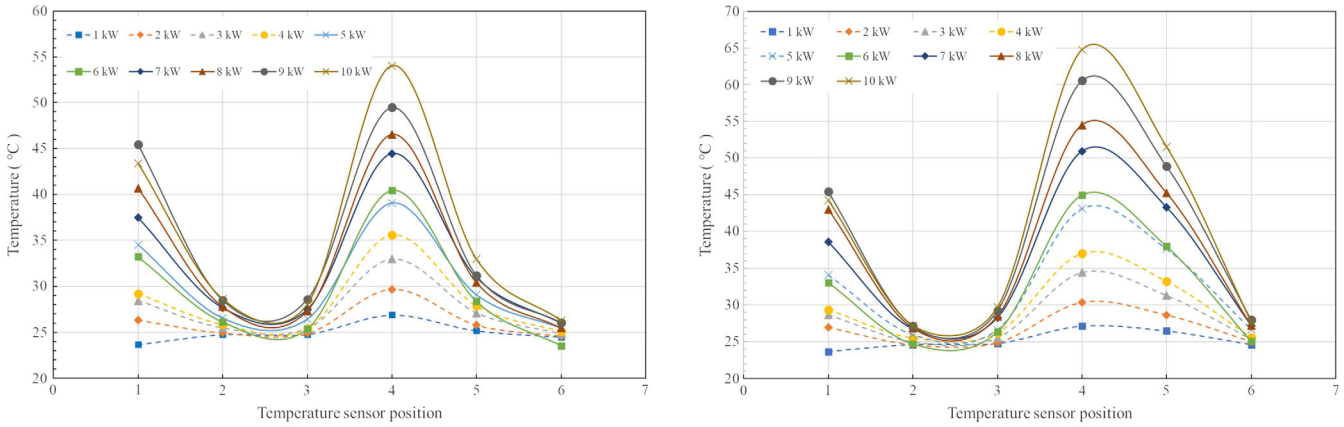

FIG. 16. Temperature distribution of FPCs with the rf power ranging from 1 to 10 kW in SW mode for the upstream coupler (a) and the downstream coupler (b).

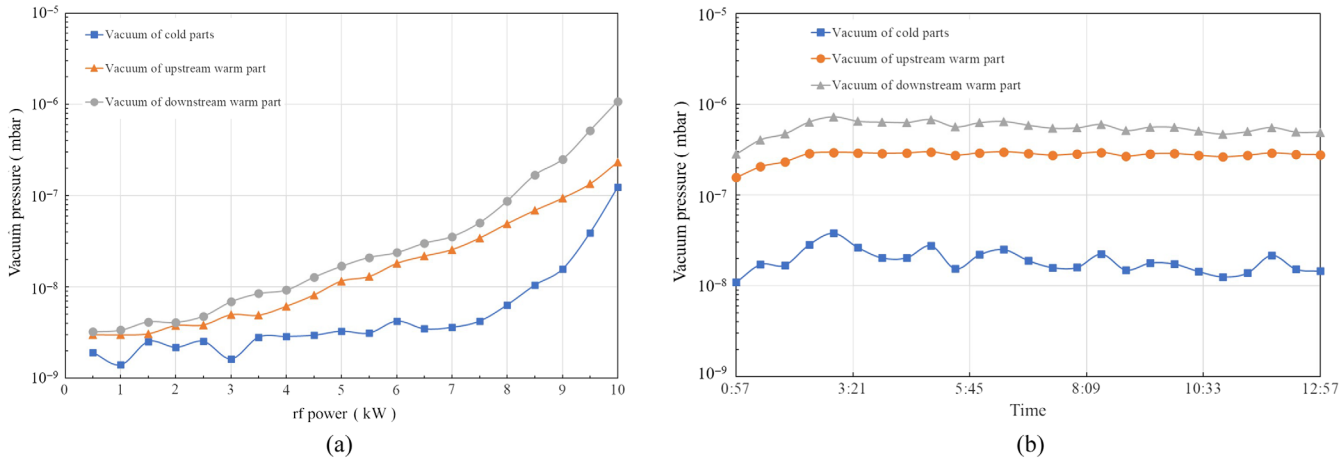

FIG. 17. The vacuum pressure of the warm parts and cold assembly with the power ranging from 1 to 10 kW in SW mode (a), and the vacuum pressure variation during the 12 h of operation at 10 kW (b).

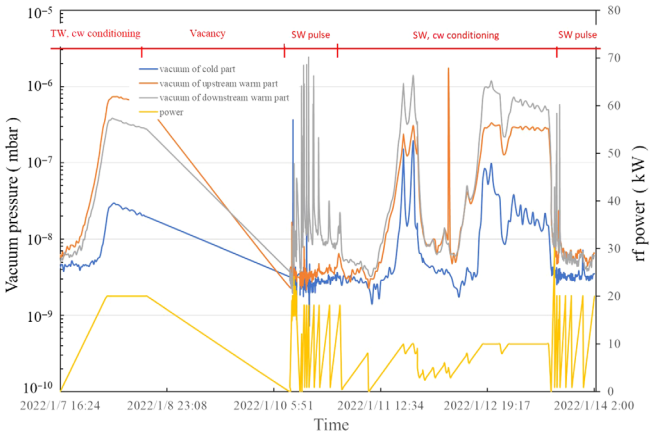

FIG. 18. The rf power test history curves for a pair of 1.3 GHz coupler prototypes.

power tests, we flowed air through the waveguides attached to the coupler to cool the warm windows, and two fans were used to cool the cold parts of the couplers to improve power handling.

IV. CONCLUSIONS AND OUTLOOKS

The SHINE 8-GeV superconducting rf electron Linac will use 600 1.3 GHz FPCs that are based on the TTF-III 1.3 GHz coupler design with some modifications for cw operation with input power up to 7 kW. The coupler modifications are basically the same as those used for the LCLS-II couplers except for the welding procedures. The first batch of 26 coupler prototypes from three domestic manufacturers was rf high power tested at room temperature. Prior to the manufacturing of the prototypes, key processes were qualified including high RRR copper plating, vacuum brazing of the ceramic rf windows, EBW, and TiN coating. All of the coupler prototypes passed the rf

high power conditioning requirements at 14 kW cw TW and 7 kW cw SW. Even higher power levels were demonstrated at 20 kW cw TW and 10 kW cw SW, which is a good validation of the manufacturing process and means that the couplers can be used for accelerator operation with higher beam current. In summary, we have established workmanship standards and acceptance criteria as a result of a collaborative effort over the years with domestic manufacturers. Improvement of the surface treatments and assembling procedures and reduction in the rf conditioning time will be our principal focus in future investigations. In addition, an automatic rf test bench has been installed and is currently being used. Its conditioning algorithm will continue to be optimized to get the best balance of processing speed and safety.

ACKNOWLEDGMENTS

We acknowledge all the people involved in the manufacturing of SHINE 1.3 GHz FPC prototypes. We are grateful to Dr. Li-Xin Yin, Dong Wang, and Yi-Yong Liu of Shanghai Advanced Research Institute, CAS, for their suggestions and support regarding the 1.3 GHz FPCs research. We are especially grateful to Dr. Denis Kostin of DESY for his long-term help and guidance in our work. This work was supported by Shanghai Municipal Science and Technology Major Project (Grant No. 2017SHZDZX02).

[1] Z. T. Zhao, C. Feng, and K. Q. Zhang, Two-stage EEHG for coherent hard X-ray generation based on a superconducting Linac, Nucl. Sci. Tech. **28**, 117 (2017).

[2] Z. Y. Zhu *et al.*, SCLF: An 8-GeV CW SCRF Linac-Based X-ray FEL Facility in Shanghai, in *Proceedings of the 38th International Free Electron Laser Conference, FEL2017, Santa Fe, NM, 2017* (JACoW, Geneva, Switzerland, 2017), pp. 182–184.

[3] B. Dwersteg *et al.*, TESLA RF power couplers development at DESY, in *Proceedings of the 10th Workshop on RF Superconductivity, SRF2001, Tsukuba, Japan* (KEK, Tsukuba, Japan, 2001), pp. 443–447, https://accelconf.web.cern.ch/srf01/papers/pt001.pdf.

[4] C. G. Maiano *et al.*, Validation of the superconducting 3.9 GHz cavity package for the European X-ray Free Electron Laser, Phys. Rev. Accel. Beams **20**, 042005 (2017).

[5] Z. Y. Ma and J. F. Chen, Design optimization of 3.9 GHz fundamental power coupler for the SHINE project, Nucl. Sci. Tech. **32**, 132 (2021).

[6] D. Kostin, E-XFEL input coupler design and simulations, Visit report of IRDA delegation at DESY (2016), https://bib-pubdb1.desy.de/record/312081/files/IRDA-Visit_XFEL_coupler_Kostin.pdf.

[7] C. Adolphsen *et al.*, Modified TTF-3 couplers for LCLS-II, in *Proceedings of SRF2015, Whistler, BC, Canada, 2015* (JACoW, Geneva, Switzerland, 2015), pp. 1306–1308.

[8] W. Kaabi *et al.*, Power couplers for XFEL, in *Proceedings of the 4th International Particle Accelerator Conference, IPAC-2013, Shanghai, China, 2013* (JACoW, Shanghai, China, 2013), https://accelconf.web.cern.ch/IPAC2013/papers/wepwo001.pdf.

[9] J. N. Galayda, The new LCLS-II Project: Status and challenges, in *Proceedings of the 27th International Linear Accelerator Conference, LINAC2014, Geneva, Switzerland* (JACoW, Geneva, Switzerland, 2014), pp. 404–408, https://accelconf.web.cern.ch/LINAC2014/papers/tuioa04.pdf.

[10] Z. Y. Ma *et al.*, High RF power tests of the first 1.3 GHz fundamental power coupler prototypes for the SHINE project, Nucl. Sci. Tech. **33**, 10 (2022).

[11] W. D. Moeller, Industrialization process for XFEL power couplers and volume manufacturing, in *Proceedings of SRF 2007* (Peking University, Beijing, China, 2007), pp. 734–739, https://accelconf.web.cern.ch/srf2007/PAPERS/TH202.pdf.

[12] H. Guler *et al.*, XFEL couplers RF conditioning at LAL, in *Proceedings of 7th International Particle Accelerator Conference, IPAC2016, Busan, Korea* (2016), pp. 2125–2127, https://accelconf.web.cern.ch/ipac2016/papers/wepmb006.pdf.

[13] A. S. Dhavale and K. C. Mittal, Multipacting analysis of power coupler for SC cavity, Nucl. Instrum. Methods Phys. Res., Sect. A **677**, 25 (2012).

[14] J. Lorkiewicz *et al.*, Surface TiN coating of TESLA couplers as an antimultipactor remedy, in *Proceedings of the 10th workshop on RF superconductivity, Tsukuba, Japan* (2001), pp. 448–452, https://accelconf.web.cern.ch/srf01/papers/pt002.pdf.

[15] W. Kaabi *et al.*, Titanium nitride coating as a multipactor suppressor, in *Proceedings of the International Particle Accelerator Conference, Kyoto, Japan* (ICR, Kyoto, 2010), pp. 2887–2889, https://accelconf.web.cern.ch/IPAC10/papers/wepec002.pdf.

[16] X. Singer *et al.*, Properties and structure of electrodeposited copper layers in parts of the TTF main coupler, in *Proceedings of the 11th Workshop on RF Superconductivity, SRF2003, Lübeck/Travemünder, Germany* (2003), pp. 652–654, https://accelconf.web.cern.ch/SRF2003/papers/thp18.pdf.

[17] L. Xiao *et al.*, TTF3 power coupler thermal analysis for LCLS-II CW operation, in *Proceedings of 6th International Particle Accelerator Conference, IPAC2015, Richmond, VA* (JACoW, Geneva, Switzerland, 2015), pp. 3503–3505, https://accelconf.web.cern.ch/IPAC2015/papers/wepwi007.pdf.

[18] M. Fouaidy and N. Hammoudi, RRR of copper coating and low temperature electrical resistivity of material for TTF couplers, Physica (Amsterdam) **441C**, 137 (2006).

[19] Z. Q. Lin *et al.*, Development of a movable standing wave resonant test system for fundamental power couplers with an extraordinary power gain, Phys. Rev. Accel. Beams **25**, 012001 (2022).

[20] H. Jenhani, T. Garvey, and A. Variola, RF conditioning studies of input power couplers for superconducting cavities operating in pulsed mode, Nucl. Instrum. Methods Phys. Res., Sect. A **595**, 549 (2008).

[21] H. Jenhani *et al.*, Developments in conditioning procedures for the TTF-III power couplers, in *Proceedings of the 10th European Particle Accelerator Conference, Edinburgh, Scotland, 2006* (EPS-AG, Edinburgh, Scotland, 2006), pp. 399–401, https://accelconf.web.cern.ch/e06/PAPERS/MOPCH147.PDF.

[22] J. Knobloch *et al.*, CW operation of the TTF-III input coupler, in *Proceedings of the 21st Particle Accelerator Conference, Knoxville, TN, 2005* (IEEE, Piscataway, NJ, 2005), pp. 3292–3294, https://accelconf.web.cern.ch/p05/PAPERS/TPPT054.PDF.

[23] N. Solyak, I. Gonin, A. Gressellino *et al.*, Results of the cavity integrated tests in horizontal test stand at FNAL, LCLS-II Technical Note TN-15–43, 2015, https://www-lcls.slac.stanford.edu/web/technotes/LCLS-II-TN-15-43.pdf.